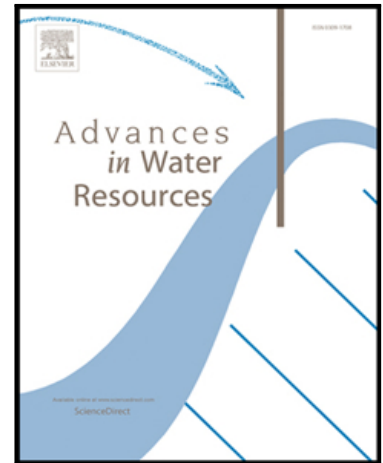


Journal Pre-proof

Impact of multiple uncertainties on gravimetric variations across randomly heterogeneous aquifers during pumping

Fadji Zaoua Maina , Alberto Guadagnini , Monica Riva

PII: S0309-1708(21)00133-0
DOI: <https://doi.org/10.1016/j.advwatres.2021.103978>
Reference: ADWR 103978



To appear in: *Advances in Water Resources*

Received date: 15 January 2021
Revised date: 17 May 2021
Accepted date: 3 June 2021

Please cite this article as: Fadji Zaoua Maina , Alberto Guadagnini , Monica Riva , Impact of multiple uncertainties on gravimetric variations across randomly heterogeneous aquifers during pumping, *Advances in Water Resources* (2021), doi: <https://doi.org/10.1016/j.advwatres.2021.103978>

This is a PDF file of an article that has undergone enhancements after acceptance, such as the addition of a cover page and metadata, and formatting for readability, but it is not yet the definitive version of record. This version will undergo additional copyediting, typesetting and review before it is published in its final form, but we are providing this version to give early visibility of the article. Please note that, during the production process, errors may be discovered which could affect the content, and all legal disclaimers that apply to the journal pertain.

© 2021 Published by Elsevier Ltd.

Highlights

- Analyses of gravity changes while pumping in 3D randomly heterogeneous aquifers
- Probability distributions of head and gravimetric variations during well operation
- Randomly heterogeneous domains consider uncertain geostatistical system descriptors
- The variance of heterogeneous fields affects mean and variance of gravity changes
- The correlation scale of the field affects extreme values of gravity changes

Journal Pre-proof

**Impact of multiple uncertainties on gravimetric variations across randomly
heterogeneous aquifers during pumping**

Fadji Zaoua Maina^{1,2}, Alberto Guadagnini^{3,4}, Monica Riva^{3,4}

¹NASA Goddard Space Flight Center, Hydrological Sciences Laboratory, Code 617,
Greenbelt, Maryland, USA

²Universities Space Research Association, Goddard Earth Sciences Technology and Research
Studies and Investigations, Columbia, Maryland, USA

³Dipartimento di Ingegneria Civile e Ambientale (DICA), Politecnico di Milano, Piazza L. Da
Vinci, 32, 20133 Milano, Italy

⁴Department of Hydrology and Atmospheric Sciences, University of Arizona, Tucson,
Arizona, USA

Abstract

We evaluate the relative importance of the uncertainty related to parameters characterizing partially saturated groundwater flow on head and gravity changes associated with pumping tests taking place in homogeneous and heterogeneous porous media. We frame our study in a Global Sensitivity Analysis setting and assess the way imperfect knowledge of such parameters influences the probability distribution (pdf) of head and gravimetric variations recorded during well operation. We rely on a set of detailed computational analyses and conceptualize uncertain model parameters as random quantities. Randomly heterogeneous domains are treated by considering main geostatistical descriptors (i.e., variance and correlation scale) of three-dimensional spatial distributions of system properties as affected by uncertainty. We quantify the effects of the latter on the resulting pdf of (ensemble) mean and variance of head and gravity changes through a numerical Monte Carlo approach. While all uncertain parameters are influential to gravity changes in both homogeneous and randomly heterogeneous scenarios, consistent with the integral nature of gravity observations, our study enables us to quantify their relative importance. Values of Ensemble mean and variance of head and gravity changes associated with randomly heterogeneous fields are generally more influenced by the variance rather than by the correlation scale of the spatially heterogeneous parameters considered. Uncertainty in the correlation scale is more influential to the shape, and hence on extreme values, of the probability distribution of these moments.

1. Introduction

Aquifer characterization commonly relies on several types of data and investigation approaches. In the context of hydrogeological analyses, for example, pumping tests are performed with the main aim of assessing hydraulic conductivity and storage capacity from drawdown observations. As hydrological systems are characterized by heterogeneity as well as temporal dynamics which are driven by diverse physical mechanisms, precise identification of the relative importance of each system parameter on target state variables (such as, e.g., hydraulic head changes) is remarkably challenging. In this context, joint use of hydrogeological data and geophysical quantities embedding information about variations of water mass stored in the system can improve our ability to characterize hydrodynamic aquifer parameters in heterogeneous system settings (Bevan et al., 2003; Rizzo et al., 2004; Andersen et al., 2005; Andersen and Hinderer, 2005; Straface et al., 2007).

Among these types of observations, gravimetric data are widely being considered to assist aquifer system characterization. Their increased use is based on the observation that gravimetric variations can be related to the displacement of water masses and mass variations taking place across the duration of pumping tests. These tests can then potentially give rise to gravity changes of several μGal (Blainey et al., 2007; Damiata and Lee, 2006; Maina and Guadagnini, 2018). In this sense, the use of gravimetric variation data in hydrological sciences is very attractive because these data can easily be obtained through modern devices which are associated with a high precision system capable of detecting also contained changes in gravity (e.g., about $3\mu\text{Gal}$) that correspond in turn to head changes of few centimeters (e.g., Jacob et al., 2008).

Gravity changes in aquifer systems have been analyzed in several studies, which were mainly concerned on characterizing storage properties (e.g., Montgomery, 1971; Pool and Eychaner, 1995; Tapley et al., 2004; Pool, 2008; Gehman et al., 2009; Hinderer et al., 2009; Jacob et al., 2008, 2009, 2010; Christiansen et al., 2011; Pfeffer et al., 2011). Some works

have specifically addressed the study of gravimetric variations associated with the operation of a pumping well in unconfined aquifers (e.g., Damiata and Lee, 2006; Blainey et al., 2007; Herckenrath et al., 2012; González- Quirós et al., 2014; Fernández-Álvarez et al., 2016). These studies have highlighted that gravimetric data (when coupled with hydrological or hydrogeological observations) can provide valuable information to guide assessment of hydrodynamic parameters (notably, storage properties). Maina and Guadagnini, (2018) rely on Global Sensitivity Analysis (GSA) and show that gravimetric data potentially contain information about several hydrodynamic system parameters while showing highest sensitivity to specific yield and storage. These authors rely on the three-dimensional analytical solution developed by Mishra and Neuman (2011) that embeds the richness of phenomena driving flow dynamics through unsaturated and saturated zones in a porous domain. Due to the complexities of the coupled unconfined/confined systems analyzed, the above mentioned analytical solution includes several approximations and assumptions, including, e.g., spatial uniformity of aquifer attributes (see also, e.g., Mishra and Neuman, 2010, 2011, and references therein).

Here, we study gravity changes associated with a pumping test. We ground our work on a suite of systematic and detailed computational studies considering homogeneous and randomly heterogeneous domains within which partially saturated flow evolves in time. We rely on a robust and efficient numerical model that allows solving the Richards equation (Richards, 1931) in three dimensional systems through a mixed hybrid finite element scheme (Chiang et al., 1989; Chavent and Roberts, 1991; Bergamaschi and Putti, 1999; Farthing et al., 2003; Bause and Knabner, 2004; Farhloul and Serghini Mounim, 2005; Belfort et al., 2009; Fahs et al., 2009), temporal integration being performed via the method of lines whose effectiveness has been documented in several works (Miller et al., 1998; Tocci et al., 1997; Williams et al., 2000; Fahs et al., 2009).

While recognizing that model parameters are typically imperfectly known and affected by uncertainty, we (i) conceptualize these as random quantities and (ii) quantify their relative degree of importance on target model outputs, i.e., head and gravity changes. We set our study in the context of a GSA framework, enabling us to (i) quantify relationships between model inputs and outputs (Homma and Saltelli, 1996; Sarrazin et al., 2016) and (ii) assess the way parametric uncertainties propagate to model outputs. Together with analyses relying on the classical Sobol' indices, which are variance-based quantities and assist defining the way uncertain model parameters affect a model output variance (see, e.g., Sobol, 1993; Homma and Saltelli 1996; Archer et al., 1997; Marrel, 2008; Sudret, 2008; Crestaux et al., 2009; Saltelli et al., 2010; Razavi and Gupta, 2015; Sarrazin et al., 2016), we further consider the sensitivity metrics recently proposed by Dell'Oca et al. (2017). The latter enable one to evaluate the contribution of model parameters to the probability density function of model outputs, as rendered through its associated statistical moments. When considering spatially heterogeneous domains, we treat system attributes as (second-order stationary) three-dimensional random fields and study the influence of imperfect knowledge of the corresponding key geostatistical descriptors (i.e., variance and correlation scale) on the uncertainty in the statistical moments (mean and variance) of head and gravity changes evaluated through a numerical Monte Carlo approach.

The work is organized as follows. Section 2 illustrates the key elements of the theoretical background, approaches and methodologies employed in the analysis. The description of the numerical setup and homogeneous and heterogeneous scenarios examined is included in Section 3. Key results are summarized in Section 4, followed by our main conclusions.

2. Mathematical Framework

2.1. Flow in variably saturated porous media

We consider transient partially saturated flow in a non-deformable porous medium governed by the following mass conservation equation for the water phase,

$$\frac{\partial \theta}{\partial t} + \frac{S_s}{\phi} \theta \frac{\partial h}{\partial t} + \nabla \cdot \mathbf{q} = f \quad (1)$$

where $S_s = \beta \rho_w g \phi$ [L^{-1}] is specific storage; ρ_w [ML^{-3}] is water density, β [$M^{-1}L^{-1}T^{-2}$] is the coefficient of compressibility of water (i.e., $\beta = \rho_w^{-1} \partial \rho_w / \partial p$, p denoting pressure); g [LT^{-2}] is gravity, ϕ [-] is porosity; h [L] is hydraulic head; θ [-] is volumetric water content; f [T^{-1}] represents a sink/source term; t [T] is time; and \mathbf{q} [LT^{-1}] is water specific discharge given by

$$\mathbf{q} = -k \mathbf{K}_s \cdot \nabla h \quad (2)$$

\mathbf{K}_s [LT^{-1}] and k [L^2] being absolute (i.e., at full saturation, $\theta = \phi$) and relative hydraulic conductivity, respectively. Relative hydraulic conductivity is a function of pressure head, $\psi = p / (g \rho_w) = h - z$, where z is elevation. Here, we employ the Gardner exponential model (Gardner et al., 1958) to describe the relationship $k = k(\psi)$, i.e.,

$$k = \begin{cases} e^{-a_k(\psi_k - \psi)} & \psi \leq \psi_k \\ 1 & \psi > \psi_k \end{cases} \quad (3)$$

where $a_k \geq 0$ is a constant (typically a function of the pore size distribution of the medium) and ψ_k is a pressure head above which $k = 1$ and (usually) coincides with the air entry pressure head, ψ_a . The volumetric water content is evaluated as (e.g., Mishra and Neuman, 2011)

$$\theta = \theta_r + S_y \begin{cases} e^{-a_c(\psi_a - \psi)} & \psi \leq \psi_a \\ 1 & \psi > \psi_a \end{cases} \quad (4)$$

where $a_c \geq 0$ is the water retention curve parameter; θ_r is residual water content, and $S_y = \phi - \theta_r$ is specific yield.

We evaluate the flow field in three dimensions through a Eulerian-type method. Numerical solutions based on the mixed form of (1) are well known to be associated with conservative properties (Celia et al., 1990). However, this form cannot be applied when considering higher order numerical integration schemes, such as the method of lines (Miller et al., 1998) which has been proven to be efficient and to provide accurate results (Fahs et al., 2009). Therefore, we rewrite (1) in the corresponding pressure form as

$$\left(C(\psi) + \frac{S_s}{\phi} \theta \right) \frac{\partial h}{\partial t} + \nabla \cdot \mathbf{q} = f \quad (5)$$

where $C(\psi) = d\theta / d\psi$ is the capacity coefficient. In our study we solve (5) by relying on a spatial discretization performed according to the mixed hybrid finite elements (Chavent and Roberts, 1991), temporal integration being grounded on the method of lines (Fahs et al., 2009; Tocci et al., 1997). Additional details about the numerical solution of (5) can be found, e.g., in Fahs et al. (2009).

2.2. Gravimetric Variations

Changes in water mass stored in the subsurface due to pumping give rise to gravimetric variations. Considering a gravimeter positioned at location (x_m, y_m, z_m) in a three-dimensional domain of infinite extent, one can write (Telford et al., 1990; Leirião et al., 2009)

$$\Delta g(t) = \gamma \int_{-\infty}^{\infty} \int_{-\infty}^{\infty} \int_{-\infty}^{\infty} \Delta \rho(x, y, z, t) \frac{-(z - z_m)}{r^3} dx dy dz ; \text{ with } r = \sqrt{(x - x_m)^2 + (y - y_m)^2 + (z - z_m)^2} \quad (6)$$

Here, Δg [L T^{-2}] is the variation of gravity (or gravity change) detected by the gravimeter between the initial (undisturbed) conditions and time t from the start of pumping, as a result of the variation of density $\Delta \rho$ [M L^{-3}], γ being the universal gravitational constant ($= 6.67 \times 10^{-11} \text{ N m}^2 \text{ kg}^{-2}$). Density variations $\Delta \rho$ depend on changes of water head, Δh , and water content, $\Delta \theta$, respectively taking place in the saturated and unsaturated regions according to

$$\Delta\rho \approx \rho_w \frac{S_s}{\phi} \Delta h \quad (7)$$

$$\Delta\rho \approx \rho_w \Delta\theta \quad (8)$$

2.3. Methodological Approach and Global Sensitivity Analysis

Models are inevitably associated with uncertainties stemming from our incomplete knowledge of the system, e.g., initial/boundary conditions, simplification in the mathematical description of the processes involved and lack of information resulting from the variety of space-time scales associated with the physical processes under study. Evaluation of gravity changes through the interpretive modeling framework detailed in Sections 2.1-2.2 relies on our knowledge of model parameters representing specific features of the system functioning. In this context, we explore the role of the uncertain model parameters in driving uncertainty associated with gravity changes, given the model structure adopted and considering a randomly heterogeneous porous medium. As discussed in the Introduction, we do so by relying on a Global Sensitivity Analysis (GSA) approach, the latter enabling us to quantitatively assess the relative importance of a set of (typically uncertain) model input parameters on model outputs of interest.

The well-known Sobol' indices (Sobol, 1993) rely on the decomposition of model output variance (Archer et al., 1997; Saltelli et al., 2010) and yield its expected reduction due to the knowledge of uncertain model parameters. Dell'Oca et al. (2017; 2020a, b) show that diagnosing a model by quantifying the importance of uncertain parameters relying solely on the model output variance provides at best an incomplete assessment of the way a model governs a system behavior. These authors propose an alternative and complementary approach based on the computation of (statistical) Moment-based Metrics. The latter aim at quantifying the impact of model parameter uncertainties on statistical moments governing main features of the probability density function (pdf) of model outputs. A brief illustration of Sobol' indices and Moment-based metrics is provided in Appendix A.

A drawback shared by most GSA techniques, including those illustrated above, is that they can be computationally very demanding, as a large number of Monte Carlo iterations might be required to obtain robust and stable estimates of the desired sensitivity metrics. This issue can be particularly relevant in complex settings of the kind here considered. The impact of such a barrier can be alleviated by resorting to the use of surrogate (or reduced order) models. Amongst various available alternatives, here we rely on an approximation of model outputs based on the Polynomial Chaos Expansion (PCE; Sudret, 2008; Wiener, 1938), other approaches being fully compatible with the methodological framework we consider. This technique has been successfully employed in the context of diverse Earth science settings (including, e.g., Crestaux et al., 2009; Fajraoui et al., 2011; Formaggia et al., 2012; Ciriello et al., 2013; Porta et al., 2014; Garcia-Cabrejo and Valocchi, 2014; Sudret and Mai, 2015; Bianchi Janetti et al. 2019; Patani et al., 2021).

3. Numerical set-up

We study the temporal evolution of gravity changes taking place during a pumping test in a three-dimensional heterogeneous unconfined aquifer. The exemplary domain has a planar extent of $100 \times 100 \text{ m}^2$ and a total thickness of 50 m. Initial hydraulic head is set to 40 m, i.e., the water table is initially located 10 m below the ground surface. Dirichlet ($h = 40 \text{ m}$) and Neumann (impervious) boundary conditions are set at the four lateral limits and at the bottom of the domain, respectively. A pumping well is located at the center of the domain and is screened between 22.5 and 27.5 m below ground surface. The pumping rate is constant ($Q = 5 \times 10^{-3} \text{ m}^3 \text{ s}^{-1}$) for the whole pumping period, here taken as 7 days. The pumping duration has been selected to ensure negligible impacts of the constant head boundary conditions on the target quantities of interest (see also Section 4.2). A gravimeter is placed on the ground surface at the well planar location and records the gravimetric variations induced by pumping. We remark that our selected pumping test duration as well as domain size and pumping rate

are consistent with pumping tests typically associated with unconfined systems (see, e.g., Bevan et al., 2003; Damiata and Lee, 2006; Leirião et al., 2009; Maina and Guadagnini 2018). To the best of our knowledge, systematic stochastic analyses on gravimetric variations induced by a pumping test in randomly heterogeneous aquifers are still lacking.

The domain is discretized with a uniform grid of size equal to 5 m. Increasing the refinement of the grid does not yield significant differences in the solution (not shown), the selected grid size allowing for a good balance between CPU time and numerical accuracy. We recall that the numerical model relies on the solver DLSODIS (Hindmarsh, 1982), the temporal discretization being then designed to ensure stability and accuracy of the solution.

The domain is isotropic along the horizontal (x, y) plane, the hydraulic conductivity matrix \mathbf{K}_S in (2) being fully defined by its horizontal, K_S , and vertical, K_{S_z} , components. Following Belfort et al. (2013), we set $\psi_k = \psi_a = 0$, $\theta_r = 0.1$, and $a_c = a_k$. Our state variable of interest (gravity changes computed via (6)) depends on the following five model input parameters, which are here considered to be affected by uncertainty: (i) horizontal (saturated) hydraulic conductivity, K_S ; (ii) anisotropy coefficient, $K_d = K_{S_z} / K_S$; (iii) specific storage, S_S ; (iv) specific yield, S_Y ; and (v) the Gardner model parameter, $a_k = a_c$.

Our study targets homogeneous and randomly heterogeneous aquifer systems, as described in the following subsections. For each scenario, our numerical analyses rest on a Quasi-Monte-Carlo technique (e.g., Caflisch, 1998; Niederreiter, 1992; Feil, 2009 and references therein) to sample the parameter space. Due to computational costs, we perform GSA by relying on the construction of surrogate models (based on PCEs) of all quantities of interest, as detailed in the following.

3.1. Homogeneous setting

We start by considering a homogeneous scenario (denoted as H_0) where all uncertain model parameters (e.g., K_S , K_d , S_S , S_Y , a_c) are considered as independent and identically

distributed (*i.i.d.*) random variables characterized by uniform distributions with supports listed in Table 1. The interval of variability considered for each uncertain parameter is consistent with previous studies (Damiata and Lee, 2006; Leirião et al., 2009) and has been designed to encompass coarse as well as fine aquifer geomaterials, resulting in coefficients of variations (CVs) of parameter distributions with magnitude around 50%.

We sample the parameter space via a Quasi-Monte-Carlo technique. Here, we rely on $m = 1,000$ random realizations and for each of these we evaluate the drawdown (with respect to the initial hydraulic head) in each cell j of the domain at time t , $\Delta h_i(j, t)$ (with $i = 1, \dots, m$), as well as the total variation of gravity, $\Delta g_i(t)$, via (6). The PCE approximations of $\Delta h_i(j, t)$ and $\Delta g_i(t)$ are then constructed to assist GSA. The quality of the PCE of order 4 (for the evaluation of both $\Delta h_i(j, t)$ and $\Delta g_i(t)$) has been assessed through cross-validation against the numerical solution of the full model illustrated in Sections 2.1 and 2.2 (details not shown). The sensitivity indices introduced in Section 2.3 and illustrated in Section 4 are then computed on the basis of 5,000 PCE runs.

3.2. Heterogeneous setting

This setting is designed to assess the effect of randomly heterogeneous spatial distributions of K_S , a_c , and S_S on total gravity changes, the remaining model parameters (i.e., K_d and S_Y) being treated as described in Section 3.1. We start by noting that while there is abundant literature devoted to the analysis of spatially correlated random fields of K_S , information about geostatistical characterizations of parameters a_c and S_S is rather limited (see, e.g., Guadagnini et al., 2013 and references therein). In our analysis we consider $Y = \log K_S$, $Y_{ac} = \log a_c$ and $Y_{SS} = \log S_S$ as second-order stationary and independent random processes normally distributed with mean values equal to $\mu_Y = -5$, $\mu_{Y_{ac}} = -1.69$, and $\mu_{Y_{SS}} = -4$,

respectively, corresponding to intermediate values of the ranges listed in Table 1. The random fields Y , Y_{ac} , and Y_{SS} are spatially correlated according to an exponential isotropic covariance function, its parameters (e.g., variance and correlation scale) being considered as affected by uncertainty and uniformly distributed in the range listed in Table 2. This enables us to explore the impact of low to mild heterogeneity of random fields characterized by various degrees of the strength of spatial correlation. We analyze the three diverse heterogeneous scenarios (hereafter denoted as H_1 , H_2 , and H_3) listed in Table 3. Note that H_0 can be viewed as a particular case of H_1 , H_2 , or H_3 , respectively corresponding to a scenario where the correlation scale of Y , Y_{ac} , or Y_{SS} is much larger than a characteristic length scale of the domain (i.e., it tends to infinity).

For each of these cases (i.e., for H_1 , H_2 or H_3) we perform our analyses according the following steps:

- (1) we generate n_p sets of parameters, i.e., variance and correlation scale of P (with $P = Y$ for H_1 ; Y_{ac} for H_2 ; and Y_{SS} for H_3 ; see Table 3), as well as all of the remaining (spatially homogeneous) random model parameters;
- (2) for each pair of values of variance and correlation scale we generate n spatial distributions of the corresponding random fields;
- (3) for each parameter set k (i.e., $k = 1, \dots, n_p$) and each realization i (with $i = 1, \dots, n$) we evaluate drawdown (with respect to the initial hydraulic head) at cell j and time t , $\Delta h_{k,i}(j, t)$, as well as the total variation of gravity, $\Delta g_{k,i}(t)$, via (6);
- (4) we then evaluate the Monte-Carlo based mean and variance of drawdown and total gravity change for parameter set k as

$$\mu_{\xi,k} = \frac{1}{n} \sum_{i=1}^n \xi_{k,i}; \quad \sigma_{\xi,k}^2 = \frac{1}{n} \sum_{i=1}^n \xi_{k,i}^2 - \mu_{\xi,k}^2; \quad \text{with } \xi_{k,i} = \Delta h_{k,i}(j, t), \Delta g_{k,i}(t) \quad (9)$$

We assess convergence of the quantities in (9) following Ballio and Guadagnini (2004) and obtain stable results for $n = 100$ (details not shown). A collection of $n_p = 200$ results stemming from (9) are then employed to construct surrogate models (i.e., PCE approximations of order 4) for mean and variance of drawdowns and total gravity changes for each of the three heterogeneous scenarios investigated and each time step considered. The accuracy of the surrogate models has been assessed by comparing outputs (in terms of mean and variance of drawdowns and total gravity changes) simulated by the surrogate models and by the full model (1)-(6) for randomly selected sets of parameters (details not shown). These surrogate models are finally employed to evaluate the GSA metrics described in Section 2.3.

4. Results and discussion

The analysis of our results is based on the temporal evolution of hydraulic head and total gravity changes recorded by the gravimeter positioned as described in Section 3. Hydraulic head is analyzed at a selected point (termed as point $j = A$), located at a radial distance from the well equal to 10 m and at the same depth as the well screened interval.

4.1 Hydraulic head

Figure 1a depicts the temporal evolution of the hydraulic head changes (drawdowns) at point A , $\Delta h_i(j = A, t)$, computed for each MC realization i (grey continuous curves) in the homogeneous scenario H_0 . The ensemble mean hydraulic head change, $\langle \Delta h \rangle = \sum_{i=1}^m \Delta h_i / m$, (black continuous curve), the 95% Confidence Intervals of $\langle \Delta h \rangle$ (black dashed curves) evaluated as $\langle \Delta h \rangle \pm 2\sqrt{V_{\Delta h} / m}$ (with $V_{\Delta h} = \sum_{i=1}^m (\Delta h_i - \langle \Delta h \rangle)^2 / m$), as well as the box plots computed at three selected times (representing the early, intermediate, and late behavior) are also depicted. The mean hydraulic head change displays features that are typical of an unconfined aquifer system, the shape of the curve being driven by the effects of artesian storage at early times and drainage from the unsaturated zone taking place at intermediate

times. The width of the uncertainty bounds tends to increase with time. This latter outcome is somehow in contrast with the results of Maina and Guadagnini (2018). We note that these authors base their study on the three-dimensional analytical solution of Mishra and Neuman (2011) and observe that the variance of hydraulic head changes is almost constant during early and intermediate times, and slightly increases only towards the end of the pumping period. The diverse behavior observed here is possibly related to the simplifying assumptions underlying the analytical solution of Mishra and Neuman (2011), which are not required in our numerical analyses.

Figure 2 depicts the temporal evolution of the ensemble mean, $\mu_{\Delta h,k}$ (left column) and variance $\sigma_{\Delta h,k}^2$ (right column) of head changes evaluated through (9) for each set k of input parameters across the heterogeneous scenarios H_1 , H_2 , and H_3 (grey curves). Average values

computed across the full collection of parameter values, $\langle \wp_{\Delta h} \rangle = \sum_{k=1}^{n_p} \wp_{\Delta h,k} / n_p$ (with $\wp = \mu, \sigma^2$, black continuous curve), the 95% Confidence Intervals of $\langle \wp_{\Delta h} \rangle$ (black dashed curves)

evaluated as $\langle \wp_{\Delta h} \rangle \pm 2\sqrt{V_{\wp_{\Delta h}} / n_p}$ (with $V_{\wp_{\Delta h}} = \sum_{k=1}^{n_p} (\wp_{\Delta h,k} - \langle \wp_{\Delta h} \rangle)^2 / n_p$), as well as the box plots

evaluated at three selected times are also depicted. The temporal behavior of $\langle \mu_{\Delta h} \rangle$ in the heterogeneous settings (see Fig 2a, c, and, e) is not characterized by a clear S-shaped distribution such as the one corresponding to $\langle \Delta h \rangle$ in the homogeneous scenario (see Fig. 1).

This feature is related to the observation that the duration of the early (where artesian storage effects are dominant) and intermediate/late (where drainage effects are dominant) periods varies as a function of the considered parameter set k and of the structure of the heterogeneity of the system. As such, averaging all of the curves results in a smooth temporal evolution of the mean head changes where the early and intermediate/late time effects are somehow (partially) overlapped and diluted.

The AMA indices quantify the relative importance of each uncertain model parameter to the statistical moments of the pdf of head changes (see Appendix A for a summary about the key definitions of these indices). Figure 3 (first column) depicts the temporal evolution of the AMA indices for Δh corresponding to H_0 . Uncertainty in the mean (as quantified by *AMAE*) and variance (as quantified by *AMAV* and by the traditional Sobol' indices) of Δh at early times are mainly controlled by S_s , K_s , and (albeit to a lesser extent) K_d . This behavior is consistent with a mechanism associated with storage in confined aquifers, which is linked to the elastic response of the system. As time progresses, mean and variance of Δh start to be influenced by the specific yield, S_y , and by the Gardner model parameter, a_c , whose contribution is related to drainage from the unsaturated zone, a phenomenon associated with a temporal delay between the early elastic response of the aquifer and the subsequent downward movement of the water table due to gravity drainage. The strength of the influence of S_s to the mean and variance of Δh tends to decrease with time, the relevance of K_s becoming dominant as steady-state is approached at late times. The impact of interactions among parameters on the total output variance (as quantified when the sum, over all parameters, of the total Sobol' index exceeds unity) is not negligible, a feature which is particularly evident at intermediate times. Higher order statistical moments of drawdown (skewness and kurtosis) are mainly influenced by a_c and S_y , which are seen to control the degree of symmetry and tailedness (*i.e.*, probability of extreme values) of the pdf of Δh at early and intermediate times.

Considering the heterogeneous case H_1 , close inspection of the temporal variations of the AMA and Sobol' indices related to $\mu_{\Delta h}$ (Fig. 3 second column) and $\sigma_{\Delta h}^2$ (Fig. 3 third column) reveals that, in general, the uncertainty of all studied parameters affects mean and variance of $\mu_{\Delta h}$ and $\sigma_{\Delta h}^2$ across the entire pumping operation. The sum of the total Sobol' indices attains values larger than those observed in H_0 , suggesting that the interaction amongst

uncertain model parameters is stronger in heterogeneous than in homogeneous settings. As opposed to what observed in the homogeneous case, the impact of S_s and K_s is not dominant on driving the mean of $\mu_{\Delta h}$ (and $\sigma_{\Delta h}^2$), all parameters being otherwise influential across time. This result is consistent with the previous observation that the temporal window where artesian storage effects are dominant is not significantly visible in heterogeneous media. On the other hand, S_s markedly influences the variance of $\mu_{\Delta h}$ and $\sigma_{\Delta h}^2$ at early times (see Fig. 3h-i), its impact otherwise decreasing with time. Our results further suggest that the (isotropic) correlation scale of Y is less influential than its variance for all statistical moments depicted in Fig. 3 (second and third column) but skewness and kurtosis of $\sigma_{\Delta h}^2$.

Results associated with the total Sobol' and the *AMAV* indices are not always in agreement. For example, while the analysis of Sobol' indices (Fig. 3e, f) would suggest that all parameters contribute to the variance of $\mu_{\Delta h}$ and $\sigma_{\Delta h}^2$ (with an overall dominance of S_s and σ_Y^2), inspection of *AMAV* (Fig. 3h, i) indicates that the variance of $\mu_{\Delta h}$ and $\sigma_{\Delta h}^2$ is (i) not influenced by the uncertainty of λ_Y , and (ii) only minimally influenced by a_c , and S_Y . The differences detected between the Sobol' and *AMAV* indices about the impact of parameters λ_Y , a_c and S_Y can be explained by noting that these contribute to the variance of $\mu_{\Delta h}$ and $\sigma_{\Delta h}^2$ only jointly with other model parameters (this feature being captured by the total Sobol' index), their variability alone not being influential to the overall variance of the quantities analyzed (note that this latter feature is the key element captured by *AMAV*).

Skewness and kurtosis of $\mu_{\Delta h}$ are influenced by all parameters, the most influential quantities being the Gardner model parameter a_c , the specific yield S_Y , and the parameters related to the spatially heterogeneous random field of K_s (i.e., λ_Y and σ_Y^2). One can note that the sum of the *AMA γ* and *AMA k* indices for $\mu_{\Delta h}$ consistently increases with time, thus

highlighting that the impact of parameter uncertainties on the shape of the pdf of $\mu_{\Delta h}$ increases with time. Otherwise, when considering $\sigma_{\Delta h}^2$ our results show that (i) values of $AMA\gamma$ remain (approximately) constant with time, while (ii) the sum of $AMAK$ contributions displays a marked peak at intermediate times, which is mainly due to the impact of a_c , to then decrease as time progresses.

The analysis of the heterogeneous settings H_2 and H_3 shows results of similar quality to those illustrated for H_1 (not shown).

4.2 Total Gravity Changes

Figure 4 depicts the temporal evolution of the total gravity change, $\Delta g_i(t)$, computed for each MC realization i (grey continuous curves) in the homogeneous setting H_0 . The ensemble mean total gravity change, $\langle \Delta g \rangle = \sum_{i=1}^m \Delta g_i / m$, (black continuous curve), the 95% Confidence Intervals of $\langle \Delta g \rangle$ (black dotted curves) evaluated as $\langle \Delta g \rangle \pm 2\sqrt{V_{\Delta g} / m}$ (with $V_{\Delta g} = \sum_{i=1}^m (\Delta g_i - \langle \Delta g \rangle)^2 / m$), as well as the box plots related to three selected times are also depicted. The mean gravity change increases nearly exponentially with time, as do the associated uncertainty bounds. A similar behavior is exhibited in the heterogeneous test cases, as shown in Fig. 5 where we depict the temporal evolution of (i) the ensemble mean, $\mu_{\Delta g,k}$ (left column, grey curves), and variance, $\sigma_{\Delta g,k}^2$ (right column, grey curves), evaluated for each set k of individual input parameters, and (ii) their average counterparts evaluated across the full set of parameters, i.e., $\langle \mu_{\Delta g} \rangle$ (left column, black continuous curves) and $\langle \sigma_{\Delta g}^2 \rangle$ (right column, black continuous curves), together with their 95% Confidence Intervals (black dashed curve) and box plots at three selected times.

The sample pdf associated with the total gravity changes recorded at selected times in H_0 (Fig. 6) displays near-exponential tails, a result which is also consistent with the findings of Maina and Guadagnini (2018). It is noted that, as time increases, some combinations of the uncertain system parameters can give rise to total gravity changes largely exceeding $3 \mu\text{Gal}$ with non-negligible probability. These values are potentially detectable considering the accuracy of typically employed gravimeters (Herckenrath et al., 2012; Jacob et al., 2008, 2009, 2010). This result is promising as it implies that one can potentially identify gravimetric variations induced by mass changes following pumping under specific settings, corresponding to given combinations of aquifer parameter values.

The empirical pdfs of $\mu_{\Delta g}$ and $\sigma_{\Delta g}$ are depicted in Fig. 7. Values of $\mu_{\Delta g}$ are typically lower than (approximately) $5 \mu\text{Gal}$ for H_1 , while they can be as high as about $10 \mu\text{Gal}$ for H_2 and H_3 , while $\sigma_{\Delta g}$ is smaller than $5 \mu\text{Gal}$ in all cases. Uncertainty and heterogeneity associated with parameters a_c and S_s shows (overall) similar effects on the resulting pdf of $\mu_{\Delta g}$, while uncertainty in the parameters characterizing the spatial distribution of K_s (as seen in H_1) yields pdfs of $\mu_{\Delta g}$ displaying higher peaks and smaller tails than their counterparts observed in H_2 and H_3 . Otherwise, pdfs of $\sigma_{\Delta g}$ are quite similar across the heterogeneous cases (albeit somehow longer tails can be observed in H_1 with respect to H_2 and H_3 at early and intermediate times).

Focusing on the homogeneous case, we then investigate how the statistical moments of Δg vary as information about the uncertain model parameters ($p_i = S_s, K_d, a_c, S_y, \text{ or } K_s$) becomes available. Figure 8a depicts the values of the mean of total gravity changes, $\langle \Delta g | p_i \rangle$, at the end of the temporal simulation window (7 days) as a result of conditioning to the knowledge of given values of each of the uncertain parameters. The unconditional mean $\langle \Delta g \rangle$

(horizontal thin line) is also depicted. Corresponding depictions for conditional variance, $V[\Delta g | p_i]$, skewness, $\gamma[\Delta g | p_i]$, and kurtosis, $k[\Delta g | p_i]$, of Δg are displayed in Fig. 8b, c, and d, respectively. Note that the interval of variation of each model parameter is here normalized to span the range [0, 1] for graphical representation purposes. Conditioning on increasing values of S_y causes the mean of Δg to monotonously increase in a quasi-linear fashion. This behavior is consistent with the structure of (6), (8), and (4), according to which variations of gravity mainly depend on corresponding variations in density, $\Delta\rho$, that increases linearly with S_y . Conditional values of mean Δg decrease with increasing K_s . This is related to the observation that the action of K_s on gravity changes is seen in (7) through hydraulic head changes (or variation of water content). Low values of K_s yield marked head changes in the unsaturated and saturated zones close to well, which are in the proximity of the gravimeter location, hence resulting in significant gravity changes. Otherwise, conditional mean values of Δg tend to increase with the anisotropy coefficient K_d and attain their largest value for isotropic conductivity systems (i.e., when $K_d = 1$). This is consistent with the observation that changes in water mass in the unsaturated zone (inducing gravity variations) tend to increase with K_d .

Values of $\langle \Delta g | a_c \rangle$ are lowest for values of a_c close to the lower and upper boundaries of the corresponding range of variability. This result is a consequence of the observation that the Gardner model parameter acts on both relative hydraulic conductivity (see (3)) and water content (see (4)). Large values of a_c (a) correspond to a very poorly permeable unsaturated zone, thus providing less water to the saturated zones, i.e., leading to small values of Δg ; and (b) hamper the ability of the unsaturated zone to store water, thus enhancing drainage towards the saturated zone, i.e. yielding large values of Δg . A reverse competition between these

effects, yielding a similar net result, takes place for small values of a_c . Due to these contrasting effects, mass variations (and hence gravity changes) are highest for intermediate values of a_c . Conditional values of total gravity change variance (Fig. 8b) display patterns similar to those detected for the corresponding mean values.

Unconditional values of skewness and kurtosis of Δg are larger than 2 and 6, respectively, highlighting the presence of long right tailing and high peakedness of the pdf of Δg (see Fig. 8c-d and Fig. 6). Conditioning leads to a decrease of the peak and of the tailing of the pdf, this being particularly manifest for small values of S_y and/or intermediate values of K_d . Otherwise, conditioning on K_s always yields tails of the pdf which are lighter than Gaussian. We further note that the conditional kurtosis is virtually independent of the values of K_s in the selected range of variability.

All uncertain parameters (albeit at differing extents) influence gravity changes in all (homogeneous and heterogeneous) scenarios, as quantified through the GSA metrics depicted in Figs. 9 (for Δg and $\mu_{\Delta g}$) and 10 (for $\sigma_{\Delta g}^2$). This result is in line with the integral nature of the gravity change, which reflects the overall response of the aquifer system and accounts for the totality of the processes taking place at diverse spatial locations.

The overall value of the *AMAE* index (which is given by the sum of the individual contribution of each model parameter) decreases during early times and then increases until the end of the pumping period (see Fig. 10a-c) for H_0 , H_1 , and (to a lesser extent) H_2 , to denote that the impact of the uncertainty in model parameters on the mean of Δg and of $\mu_{\Delta g}$ (i.e., on $\langle \Delta g \rangle$ and $\langle \mu_{\Delta g} \rangle$) is increasingly strong as time progresses. Otherwise, the total value of *AMAE* does not vary significantly with time in H_3 , suggesting that the uncertain parameters (globally) affect the uncertainty of $\mu_{\Delta g}$ in a similar way at all times. Analyzing the

contribution of each parameter to $AMAE$ (see Fig. 10a-d), we note that the impact of K_s (or of the parameters controlling the spatial distribution of K_s in H_1) increases with time, this parameter being recognized as the most influential one to $\langle \Delta g \rangle$ and $\langle \mu_{\Delta g} \rangle$. With reference to the remaining parameters, it is observed that: (i) in H_0 (Fig. 10a) the uncertainty associated with $\langle \Delta g \rangle$ significantly depends also on S_s , a_c , and K_d in a fashion that is near-constant with time while the strength of the impact of S_y on $\langle \Delta g \rangle$ increases with time; (ii) in H_1 (Fig. 10b) all parameters are influential to $\langle \mu_{\Delta g} \rangle$, their impact increasing with time; (iii) in H_2 (Fig. 10c) and H_3 (Fig. 10d) the impact of S_s (or of the uncertainty of the parameters characterizing the spatial distribution of S_s) on $\langle \mu_{\Delta g} \rangle$ is negligible.

The importance of the system parameters on the variance of Δg , $V[\Delta g]$, and of $\mu_{\Delta g}$, $V[\mu_{\Delta g}]$, is seen to vary with time in H_0 and (to a lesser extent) H_1 as one can infer from the analysis of the Sobol' indices depicted in Fig. 9e-f. The total Sobol' index, which imbues effects of parameter interactions contributing to $V[\Delta g]$ and $V[\mu_{\Delta g}]$, tends to decrease (at early times for H_0 and H_1), increase (during intermediate times for H_1) or remain constant (at late times for $H_0 - H_1$, at all times for $H_2 - H_3$) with time. All of the heterogeneous scenarios are characterized by larger values of the total Sobol' index when compared against H_0 , documenting an enhanced joint effect of parameter uncertainty in the former than in the latter setting. Otherwise, the overall value of the $AMAV$ index (Fig. 9i-l), which quantifies the impact of the variability of each individual parameter to the overall variance of Δg and $\mu_{\Delta g}$, is generally smaller in the heterogeneous scenarios than in their homogeneous counterpart.

The total Sobol' indices related to Δg and $\mu_{\Delta g}$ in H_0 and H_1 suggest that the contributions of all parameters decrease during early times, S_s being the sole exception to

this behavior. Notably, the variance of Δg recorded at late times is practically insensitive to S_s and K_d (see Fig. 9e, i) in H_0 . Otherwise, system heterogeneity promotes the joint influence of all parameters to the variance of $\mu_{\Delta g}$ across the entire window of well operation. The contribution of each parameter to the variance of $\mu_{\Delta g}$ can be inferred by jointly analyzing the results of Figs. 9 f-h, j-l. We note that: (i) the impact of K_s is dominant in all cases, while K_d is relevant only for H_2 at late times (Fig. 9k); (ii) the remaining uncertain parameters contribute only jointly to the uncertainty associated with the variance of $\mu_{\Delta g}$ and their combined effect is always significant (Figs. 9 f-h).

Indices $AMA\gamma$ and $AMAK$ in Fig. 9, denoting the impact of parameter uncertainty on the shape of the pdf of Δg and $\mu_{\Delta g}$, exhibit a clear pattern in their time-dependent behavior only for the homogenous case H_0 . In the latter setting, all uncertain parameters but K_s influence the shape of the pdf of Δg , storage parameters (S_s and S_y) and conductivity anisotropy (K_d) being the most dominant ones in driving the skewness, and a_c and S_y governing kurtosis. Considering the heterogeneous scenarios, all parameters (including K_s) impact the shape of the pdf of $\mu_{\Delta g}$ in terms of its skewness and kurtosis.

With reference to the uncertainty in the parameters describing the (randomly heterogeneous) spatial distribution of the uncertain model attributes (K_s in H_1 , a_c in H_2 , and S_s in H_3) we note that (i) mean and variance of $\mu_{\Delta g}$ are generally more impacted by the variance than by the correlation scale of the spatially heterogeneous parameter; and (ii) the opposite occurs with reference to the shape of the pdf of $\mu_{\Delta g}$ (as measured in terms of its skewness and kurtosis).

Results for the indices evaluated for $\sigma_{\Delta g}^2$ are depicted in Fig. 10. In general, these display a pattern which is similar to the one observed in Fig. 9 for $\mu_{\Delta g}$, albeit indices related to $\sigma_{\Delta g}^2$ do not (in general) show a clear temporal trend. The most relevant differences are detected (i) with reference to H_2 and H_3 , where one can note that the impact of K_s on $AMAE$ and $AMAV$, is not dominant for $\sigma_{\Delta g}^2$, as opposed to what can be seen for $\mu_{\Delta g}$ (compare Figure 9c-d, k-l and 10b-c, h-i), or (ii) with reference to H_1 where one can note that $AMAV$ for $\sigma_{\Delta g}^2$ is significantly affected also by S_y and not only by K_s as also observed for $\mu_{\Delta g}$ (compare Figure 9j and 10g).

We recall that the pumping duration has been selected to ensure negligible impacts of the constant head boundary conditions on the target quantities of interest. Average percent differences between total gravity changes ($\Delta g(t)$) evaluated in this study and for a homogeneous domain associated with twice the lateral side start to be higher than 2% after $\sim 2 \times 10^5$ seconds and attain a large value equal to approximately 7% at the end of the considered simulation window (details not shown). This is also in line with the dependence between local values of gravity change and the distance from the gravimeter (see Eq. (7)), which is set at the well location. Otherwise, relative differences between drawdown values at point A and corresponding to these scenarios is always less than $\sim 2\%$. These results imbue us with confidence about the robustness of our study within the investigated domain. Additional studies can be planned to further characterize the influence of deterministic boundary conditions on the statistics of gravity changes for diverse values of the ratio between the domain size and the correlation scale of the randomly heterogeneous fields considered.

5 Conclusions

We analyze the impact of an incomplete knowledge about characteristic parameters of unconfined aquifers on (i) hydraulic head and (ii) gravity changes monitored during pumping

tests within homogeneous and randomly heterogeneous system. Our work leads to the following major conclusions.

1. In the homogeneous scenario, where all uncertain model parameters are considered as *i.i.d.* random variables, mean head changes are characterized by a typical S-shaped temporal pattern. This behavior is not visible when analyzing their counterparts in randomly heterogeneous media, where heterogeneity somehow shadows differences related to aquifer responses linked to early (where artesian storage effects are dominant) and intermediate/late (where drainage effects are dominant) times.
2. Consistent with the previous conclusion, global sensitivity indices, quantifying the relative importance of uncertain model parameters to statistical moments of quantities of interest, show a clear temporal behavior in the homogeneous setting, while they are (in general) fairly constant in the heterogeneous settings.
3. In the homogeneous scenario uncertainty in the mean and variance of head changes, Δh , at early times are mainly controlled by the specific storage, S_s , governing the elastic response of the system through storage, and by hydraulic conductivity, K_s . As time progresses, mean and variance of Δh start to be influenced by parameters related to drainage from the unsaturated zone (i.e., specific yield, S_y , and the Gardner model parameter, a_c). Otherwise, the analysis of the heterogeneous cases documents that the uncertainty of all considered model parameters generally affects mean and variance of head changes throughout the entire pumping operation, even as the strength of the impact of S_s tends to diminish with time. Saturated conductivity (or the parameters describing its

statistical structure) is seen to be the most influential uncertain parameter at steady-state condition for all cases.

4. The shape of the pdf of head changes (as described in terms of skewness and kurtosis) is significantly affected only by a_c and S_y in the homogeneous setting, while all parameters are important for the heterogeneous cases.
5. All uncertain parameters (albeit at differing and quantifiable extents) influence gravity changes, Δg , in all (homogeneous and heterogeneous) scenarios. This result is consistent with the observation that Δg data embed the effects of the totality of the processes taking place at diverse spatial locations in the system. The most influential parameter for the mean and variance of Δg is, in general, K_s . Otherwise, K_s does not significantly impact the shape of the pdf of Δg in the homogeneous case.
6. Considering the heterogeneous scenarios, mean and variance of head and gravity changes are generally more influenced by the variance rather than by the correlation scale of the spatially heterogeneous parameters considered. Otherwise, knowledge of the correlation scale of the random field is significantly important to constrain the shape of the pdfs of these moments, and hence their extreme values.
7. The impact of interactions among parameters on the variability of Δh and Δg , as quantified in terms of the total Sobol' indices, is not negligible, and is largest in the heterogeneous than in the homogeneous settings.

Author contribution:

- Fadji Zaoua Maina: Conceptualization; Formal analysis; Methodology; Software; Writing - original draft, Writing - review & editing.
- Alberto Guadagnini: Conceptualization; Formal analysis; Methodology; Software; Writing - original draft, Writing - review & editing.
- Monica Riva: Conceptualization; Formal analysis; Methodology; Software; Writing - original draft, Writing - review & editing; Funding acquisition.

Conflict of interest

The authors declare that they have no known competing financial interests or personal relationships that could have appeared to influence the work reported in this paper.

References

- Andersen, O.B., Hinderer, J., 2005. Global inter-annual gravity changes from GRACE: Early results. *Geophys. Res. Lett.* 32, L01402. <https://doi.org/10.1029/2004GL020948>
- Andersen, O.B., Seneviratne, S.I., Hinderer, J., Viterbo, P., 2005. GRACE-derived terrestrial water storage depletion associated with the 2003 European heat wave. *Geophys. Res. Lett.* 32, L18405. <https://doi.org/10.1029/2005GL023574>
- Archer, G.E.B., Saltelli, A., Sobol, I.M., 1997. Sensitivity measures, anova-like Techniques and the use of bootstrap. *J. Stat. Comput. Simul.* 58, 99-120. <https://doi.org/10.1080/00949659708811825>
- Ballio, F., Guadagnini, A., 2004. Convergence assessment of numerical Monte Carlo simulations in groundwater hydrology. *Water Resour. Res.* 40. <https://doi.org/10.1029/2003WR002876>
- Bause, M., Knabner, P., 2004. Computation of variably saturated subsurface flow by adaptive mixed hybrid finite element methods. *Adv. Water Resour.* 27, 565-581. <https://doi.org/10.1016/j.advwatres.2004.03.005>

- Belfort, B., Younes, A., Fahs, M., and Lehmann, F., 2013. On equivalent hydraulic conductivity for oscillation-free solutions of Richard's equation, *J. Hydrol.*, 505, 202-217, <https://doi.org/10.1016/j.jhydrol.2013.09.047>.
- Belfort, B., Ramasomanana, F., Younes, A., Lehmann, F., 2009. An Efficient Lumped Mixed Hybrid Finite Element Formulation for Variably Saturated Groundwater Flow. *Vadose Zone J.* 8, 352–362. <https://doi.org/10.2136/vzj2008.0108>
- Bergamaschi, L., Putti, M., 1999. Mixed finite elements and Newton-type linearizations for the solution of Richards' equation. *Int. J. Numer. Methods Eng.* 45, 1025-1046. [https://doi.org/10.1002/\(SICI\)1097-0207\(19990720\)45:8<1025::AID-NME615>3.0.CO;2-G](https://doi.org/10.1002/(SICI)1097-0207(19990720)45:8<1025::AID-NME615>3.0.CO;2-G)
- Bevan, M.J., Endres, A.L., Rudolph, D.L., Parkin, G., 2003. The non-invasive characterization of pumping-induced dewatering using ground penetrating radar. *J. Hydrol., Recent Advances in Aquifer Hydraulics and Their Applications to Aquifer and Vadose Zone Characterization, Remediation, and Dewatering* 281, 55-69. [https://doi.org/10.1016/S0022-1694\(03\)00200-2](https://doi.org/10.1016/S0022-1694(03)00200-2)
- Bianchi Janetti, E., Guadagnini, L., Riva, M., Guadagnini, A., 2019. Global sensitivity analyses of multiple conceptual models with uncertain parameters driving groundwater flow in a regional-scale sedimentary aquifer. *Journal of Hydrology*, 574, 544-556. <https://doi.org/10.1016/j.jhydrol.2019.04.035>
- Blainey, J.B., Ferré, T.P.A., Cordova, J.T., 2007. Assessing the likely value of gravity and drawdown measurements to constrain estimates of hydraulic conductivity and specific yield during unconfined aquifer testing. *Water Resour. Res.* 43, W12408. <https://doi.org/10.1029/2006WR005678>
- Caflisch, R.E., 1998. Monte Carlo and quasi-Monte Carlo methods. *Acta Numer.* 7, 1-49. <https://doi.org/10.1017/S0962492900002804>

- Celia, M.A., Bouloutas, E.T., Zarba, R.L., 1990. A general mass-conservative numerical solution for the unsaturated flow equation. *Water Resour. Res.* 26, 1483-1496. <https://doi.org/10.1029/WR026i007p01483>
- Chavent, G., Roberts, J.E., 1991. A unified physical presentation of mixed, mixed-hybrid finite elements and standard finite difference approximations for the determination of velocities in waterflow problems. *Adv. Water Resour.* 14, 329-348. [https://doi.org/10.1016/0309-1708\(91\)90020-O](https://doi.org/10.1016/0309-1708(91)90020-O)
- Chiang, C.Y., Wheeler, M.F., Bedient, P.B., 1989. A modified method of characteristics technique and mixed finite elements method for simulation of groundwater solute transport. *Water Resour. Res.* 25, 1541-1549. <https://doi.org/10.1029/WR025i007p01541>
- Christiansen, L., Binning, P.J., Rosbjerg, D., Andersen, O.B., Bauer-Gottwein, P., 2011. Using time-lapse gravity for groundwater model calibration: An application to alluvial aquifer storage. *Water Resour. Res.* 47, W06503. <https://doi.org/10.1029/2010WR009859>
- Ciriello, V., Di Federico, V., Riva, M., Cadini, F., De Sanctis, J., Zio E.; Guadagnini, A. 2013. Polynomial Chaos Expansion for Global Sensitivity Analysis applied to a model of radionuclide migration in randomly heterogeneous aquifers. *Stochastic Environmental Research and Risk Assessment*, 27(4): 945-954. <https://doi.org/10.1007/s00477-012-0616-7>.
- Crestaux, T., Le Maître, O., Martinez, J.-M., 2009. Polynomial chaos expansion for sensitivity analysis. *Reliab. Eng. Syst. Saf.* 94, 1161-1172. <https://doi.org/10.1016/j.res.2008.10.008>

- Damiata, B.N., Lee, T.-C., 2006. Simulated gravitational response to hydraulic testing of unconfined aquifers. *J. Hydrol.* 318, 348-359. <https://doi.org/10.1016/j.jhydrol.2005.06.024>
- Dell'Oca, A., Guadagnini, A., Riva, M., 2020a. Copula density-driven metrics for sensitivity analysis: Theory and application to flow and transport in porous media. *Advances in Water Resources* 145, 103714. <https://doi.org/10.1016/j.advwatres.2020.103714>
- Dell'Oca, A., Riva, M., Guadagnini, A., 2020b. Global Sensitivity Analysis for Multiple Interpretive Models With Uncertain Parameters. *Water Resources Research* 56, e2019WR025754. <https://doi.org/10.1029/2019WR025754>
- Dell'Oca, A., Riva, M., Guadagnini, A., 2017. Moment-based Metrics for Global Sensitivity Analysis of Hydrological Systems. *Hydrol Earth Syst Sci Discuss* 2017, 1-41. <https://doi.org/10.5194/hess-2017-90>
- Fahs, M., Younes, A., Lehmann, F., 2009. An easy and efficient combination of the Mixed Finite Element Method and the Method of Lines for the resolution of Richards' Equation. *Environ. Model. Softw.* 24, 1122-1126. <https://doi.org/10.1016/j.envsoft.2009.02.010>
- Fajraoui, N., Ramasomanana, F., Younes, A., Mara, T.A., Ackerer, P., Guadagnini, A., 2011. Use of global sensitivity analysis and polynomial chaos expansion for interpretation of nonreactive transport experiments in laboratory-scale porous media. *Water Resour. Res.* 47, W02521. <https://doi.org/10.1029/2010WR009639>
- Farhloul, M., Serghini Mounim, A., 2005. A mixed-hybrid finite element method for convection–diffusion problems. *Appl. Math. Comput.* 171, 1037-1047. <https://doi.org/10.1016/j.amc.2005.01.101>

- Farthing, M.W., Kees, C.E., Miller, C.T., 2003. Mixed finite element methods and higher order temporal approximations for variably saturated groundwater flow. *Adv. Water Resour.* 26, 373-394. [https://doi.org/10.1016/S0309-1708\(02\)00187-2](https://doi.org/10.1016/S0309-1708(02)00187-2)
- Feil B., S.K., 2009. Comparison of Monte Carlo and Quasi Monte Carlo Sampling Methods in High Dimensional Model Representation 12-17. <https://doi.org/10.1109/SIMUL.2009.34>
- Fernández-Álvarez, P.; González-Quirós, A.; Rubio-Melendi, D. 2016. Assessment of the value of microgravity to estimate the principal directions of the anisotropic transmissivity of aquifers from pumping tests: a study using a Hough Transform based automatic algorithm. *Journal of Applied Geophysics*, 134, 172- 182 <https://doi.org/10.1016/j.jappgeo.2016.09.015>
- Formaggia, L., Guadagnini, A., Imperiali, I., Lever, V., Porta, G., Riva, M., Scotti, A., Tamellini, L., 2012. Global sensitivity analysis through polynomial chaos expansion of a basin-scale geochemical compaction model. *Comput. Geosci.* 17, 25-42. <https://doi.org/10.1007/s10596-012-9311-5>
- Garcia-Cabrejo, O., Valocchi, A., 2014. Global Sensitivity Analysis for multivariate output using Polynomial Chaos Expansion. *Reliab. Eng. Syst. Saf.* 126, 25-36. <https://doi.org/10.1016/j.res.2014.01.005>
- Gardner, T.R., Gardner, W.R., Gardner, W., Gardner, W.R., Gardner, T., 1958. Some steady state solutions of the unsaturated moisture flow equation with application to evaporation from water table. <https://doi.org/10.1097/00010694-195804000-00006>
- Gehman, C.L., Harry, D.L., Sanford, W.E., Stednick, J.D., Beckman, N.A., 2009. Estimating specific yield and storage change in an unconfined aquifer using temporal gravity surveys. *Water Resour. Res.* 45, W00D21. <https://doi.org/10.1029/2007WR006096>.

- González- Quirós, A.; Fernández- Álvarez, P. 2014. Simultaneous solving of three-dimensional gravity anomalies caused by pumping tests in unconfined aquifers. *Mathematical Geosciences*, 46(6), 649- 664. <https://doi.org/10.1007/s11004-014-9539-9>.
- Guadagnini, A., Neuman, S.P., Schaap, M.G., Riva, M., 2013. Anisotropic Statistical Scaling of Vadose Zone Hydraulic Property Estimates near Maricopa, Arizona, *Water Resour. Res.*, 49, 1-17, doi:10.1002/2013WR014286.
- Herckenrath, D., Auken, E., Christiansen, L., Behroozmand, A.A., Bauer-Gottwein, P., 2012. Coupled hydrogeophysical inversion using time-lapse magnetic resonance sounding and time-lapse gravity data for hydraulic aquifer testing: Will it work in practice? *Water Resour. Res.* 48, W01539. <https://doi.org/10.1029/2011WR010411>
- Hinderer, J., de Linage, C., Boy, J.P., Gegout, P., Masson, F., Rogister, Y., Amalvict, M., Pfeffer, J., Littel, F., Luck, B., Bayer, R., Champollion, C., Collard, P., Le Moigne, N., Diamant, M., Deroussi, S., de Viron, O., Biancale, R., Lernoine, J.M., Bonvalot, S., Gabalda, G., Bock, O., Genthon, P., Boucher, M., Favreau, G., Seguis, L., Delclaux, F., Cappelaere, B., Oi, M., Descloitres, M., Galle, S., Laurent, J.P., Legchenko, A., Bouin, M.N., 2009. The GHYRAF (Gravity and Hydrology in Africa) experiment : description and first results. *J. Geodyn.* 48, 172–181. <https://doi.org/10.1016/j.jog.2009.09.014>
- Hindmarsh, A., 1982. Large ordinary differential equation systems and software. *IEEE Control Syst. Mag.* 2, 24–30. <https://doi.org/10.1109/MCS.1982.1103756>
- Homma, T., Saltelli, A., 1996. Importance measures in global sensitivity analysis of nonlinear models. *Reliab. Eng. Syst. Saf.* 52, 1–17. [https://doi.org/10.1016/0951-8320\(96\)00002-6](https://doi.org/10.1016/0951-8320(96)00002-6)

- Jacob, T., Bayer, R., Chery, J., Jourde, H., Moigne, N.L., Boy, J.-P., Hinderer, J., Luck, B., Brunet, P., 2008. Absolute gravity monitoring of water storage variation in a karst aquifer on the larzac plateau (Southern France). *J. Hydrol.* 359, 105-117. <https://doi.org/10.1016/j.jhydrol.2008.06.020>
- Jacob, T., Bayer, R., Chery, J., Le Moigne, N., 2010. Time-lapse microgravity surveys reveal water storage heterogeneity of a karst aquifer. *J. Geophys. Res. Solid Earth* 115, B06402. <https://doi.org/10.1029/2009JB006616>
- Jacob, T., Chery, J., Bayer, R., Le Moigne, N., Boy, J.-P., Vernant, P., Boudin, F., 2009. Time-lapse surface to depth gravity measurements on a karst system reveal the dominant role of the epikarst as a water storage entity. *Geophys. J. Int.* 177, 347-360. <https://doi.org/10.1111/j.1365-246X.2009.04118.x>
- Leirião, S., He, X., Christiansen, L., Andersen, O.B., Bauer-Gottwein, P., 2009. Calculation of the temporal gravity variation from spatially variable water storage change in soils and aquifers. *J. Hydrol.* 365, 302-309. <https://doi.org/10.1016/j.jhydrol.2008.11.040>
- Maina, F.Z., Guadagnini, A., 2018. Uncertainty Quantification and Global Sensitivity Analysis of Subsurface Flow Parameters to Gravimetric Variations During Pumping Tests in Unconfined Aquifers. *Water Resour. Res.* 54, 501-518. <https://doi.org/10.1002/2017WR021655>
- Marrel, A., 2008. Mise en oeuvre et utilisation du métamodèle processus gaussien pour l'analyse de sensibilité de modèles numériques : application à un code de transport hydrogéologique (Thèse de doctorat). Institut National des Sciences Appliquées de Toulouse.
- Miller, C.T., Williams, G.A., Kelley, C.T., Tocci, M.D., 1998. Robust solution of Richards' equation for nonuniform porous media. *Water Resour. Res.* 34, 2599-2610. <https://doi.org/10.1029/98WR01673>

- Mishra, P.K., Neuman, S.P., 2011. Saturated-unsaturated flow to a well with storage in a compressible unconfined aquifer. *Water Resour. Res.* 47, W05553. <https://doi.org/10.1029/2010WR010177>
- Mishra, P.K., Neuman, S.P., 2010. Improved forward and inverse analyses of saturated-unsaturated flow toward a well in a compressible unconfined aquifer. *Water Resour. Res.* 46, W07508. <https://doi.org/10.1029/2009WR008899>
- Montgomery, E.L., 1971. Determination of coefficient of storage by use of gravity measurements.
- Niederreiter, H., 1992. *Random Number Generation and Quasi-Monte Carlo Methods*. SIAM.
- Patani, S.E., Porta, G.M., Guadagnini, A., Caronni, V., Ruffo, P., 2021. Stochastic inverse modeling and parametric uncertainty of sediment deposition processes across geologic time scales, *Math. Geosc.*, 1-24, <https://doi.org/10.1007/s11004-020-09911-z>.
- Pfeffer, J., Boucher, M., Hinderer, J., Favreau, G., Boy, J.-P., de Linage, C., Cappelaere, B., Luck, B., Oi, M., Le Moigne, N., 2011. Local and global hydrological contributions to time-variable gravity in Southwest Niger. *Geophys. J. Int.* 184, 661-672. <https://doi.org/10.1111/j.1365-246X.2010.04894.x>
- Pool, D.R., 2008. The utility of gravity and water-level monitoring at alluvial aquifer wells in southern Arizona. *Geophysics* 73. <https://doi.org/10.1190/1.2978166>
- Pool, D.R., Eychaner, J.H., 1995. Measurements of aquifer-storage change and specific yield using gravity surveys. *Groundwater* 33, 425-432. <https://doi.org/10.1111/j.1745-6584.1995.tb00299.x>
- Porta, G.M., Tamellini, L., Lever, V., Riva, M., 2014. Inverse modeling of geochemical and mechanical compaction in sedimentary basins through Polynomial Chaos Expansion, *Water Resour. Res.*, 50, 12, 9414-9431, doi: 10.1002/2014WR015838

- Razavi, S., Gupta, H.V., 2015. What do we mean by sensitivity analysis? The need for comprehensive characterization of “global” sensitivity in Earth and Environmental systems models. *Water Resour. Res.* 51, 3070-3092.
<https://doi.org/10.1002/2014WR016527>
- Richards, L.A., 1931. Capillary conduction of liquids through porous medium. *J. Appl. Phys.* 1, 318–333. <https://doi.org/10.1063/1.1745010>
- Rizzo, E., Suski, B., Revil, A., Straface, S., Troisi, S., 2004. Self-potential signals associated with pumping tests experiments. *J. Geophys. Res. Solid Earth* 109, B10203.
<https://doi.org/10.1029/2004JB003049>
- Saltelli, A., Annoni, P., Azzini, I., Campolongo, F., Ratto, M., Tarantola, S., 2010. Variance based sensitivity analysis of model output. Design and estimator for the total sensitivity index. *Comput. Phys. Commun.* 181, 259-270.
<https://doi.org/10.1016/j.cpc.2009.09.018>
- Sarrazin, F., Pianosi, F., Wagener, T., 2016. Global Sensitivity Analysis of environmental models: Convergence and validation. *Environ. Model. Softw.* 79, 135-152.
<https://doi.org/10.1016/j.envsoft.2016.02.005>
- Sobol, I. M., 1993. Sensitivity estimates for nonlinear mathematical models. *Mathematical Modeling and Computation*, 1, 407-414.
- Straface, S., Fallico, C., Troisi, S., Rizzo, E., Revil, A., 2007. An inverse procedure to estimate transmissivity from heads and SP signals. *Ground Water* 45, 420-428.
<https://doi.org/10.1111/j.1745-6584.2007.00310.x>
- Sudret, B., 2008. Global sensitivity analysis using polynomial chaos expansions. *Reliab. Eng. Syst. Saf., Bayesian Networks in Dependability* 93, 964–79.
<https://doi.org/10.1016/j.res.2007.04.002>

- Sudret, B., Mai, C.V., 2015. Computing derivative-based global sensitivity measures using polynomial chaos expansions. *Reliab. Eng. Syst. Saf.* 134, 241-250. <https://doi.org/10.1016/j.ress.2014.07.009>
- Tapley, B.D., Bettadpur, S., Watkins, M., Reigber, C., 2004. The gravity recovery and climate experiment: Mission overview and early results. *Geophys. Res. Lett.* 31, L09607. <https://doi.org/10.1029/2004GL019920>
- Telford, William Murray, Telford, W. M., Geldart, L.P., Sheriff, R.E., 1990. *Applied Geophysics*. Cambridge University Press
- Tocci, M.D., Kelley, C.T., Miller, C.T., 1997. Accurate and economical solution of the pressure-head form of Richards' equation by the method of lines. *Adv. Water Resour.* 20, 1–14. [https://doi.org/10.1016/S0309-1708\(96\)00008-5](https://doi.org/10.1016/S0309-1708(96)00008-5)
- Wiener, N., 1938. The Homogeneous Chaos. *Am. J. Math.* 60, 897-936. <https://doi.org/10.2307/2371268>
- Williams, G.A., Miller, C.T., Kelley, C.T., 2000. Transformation approaches for simulating flow in variably saturated porous media. *Water Resour. Res.* 36, 923-934. <https://doi.org/10.1029/1999WR900349>

FIGURES CAPTION

Figure 1. Temporal evolution of drawdown at point A (located at a radial distance from the well equal to 10 m and at the same depth as the well screened interval) computed for each MC realization (grey curves) in the homogeneous scenario (H_0). Ensemble mean drawdown (black continuous curve), its 95% Confidence Intervals (black dashed curves) and box-plots at three selected times (in red) are also depicted.

Figure 2. Temporal evolution of $\mu_{\Delta h,k}$ (left column) and $\sigma_{\Delta h,k}^2$ (right column) evaluated at point A for each set k of input parameters (grey curves) in the heterogeneous scenarios. Average curves computed across the full collection of parameter values (black continuous curves) and their 95% Confidence Intervals (black dashed curve) as well as the box plots evaluated at three selected times (in red) are also depicted.

Figure 3. Temporal evolution of $AMAE$, Sobol', $AMAV$, $AMA\gamma$ and $AMAK$ indices associated with (i) Δh for H_0 (first column), (ii) $\mu_{\Delta h}$ for H_1 (second column) and (iii) $\sigma_{\Delta h}^2$ for H_1 (third column).

Figure 4. Temporal evolution of the total gravity change computed for each MC realization (grey curves) in the homogeneous scenario. Ensemble mean gravity change (black continuous curve), its 95% Confidence Intervals (black dashed curves) and box-plots at three selected times (in red) are also depicted.

Figure 5. Temporal evolution of $\mu_{\Delta g,k}$ (left column) and $\sigma_{\Delta g,k}^2$ (right column) evaluated for each set k of input parameters (grey curves) in the heterogeneous scenarios. Average curves

computed across the full collection of parameter values (black continuous curves) and their 95% Confidence Intervals (black dotted curve) as well as the box plots evaluated at three selected times (in red) are also depicted.

Figure 6. Sample pdf of Δg at selected times for H_0 (symbols). Exponential fitted models (dashed curves) are also shown for comparison.

Figure 7. Sample pdf of $\mu_{\Delta g}$ (top) and $\sigma_{\Delta g}$ (bottom) at selected times for the heterogeneous scenarios (symbols).

Figure 8. Conditional (a) mean, (b) variance, (c) skewness, and (d) kurtosis of Δg versus normalized model parameters p_i at time $t = 7$ days for H_0 . Corresponding unconditional moments are also shown (horizontal lines).

Figure 9. Temporal evolution of $AMAE$, Sobol', $AMAV$, $AMA\gamma$ and $AMAK$ indices associated with (i) Δg for H_0 (first column), and (ii) $\mu_{\Delta g}$ for H_1 (second column), H_2 (third column), and H_3 (last column).

Figure 10. Temporal evolution of $AMAE$, Sobol', $AMAV$, $AMA\gamma$ and $AMAK$ associated with $\sigma_{\Delta g}^2$ for H_1 (first column), H_2 (second column), and H_3 (third column).

Tables

Par	Supp	C
ameter	ort	V
s_s	$[10^{-5}$	5
$[\text{m}^{-1}]$	$- 10^{-3}]$	7%
s_y	$[10^{-2}$	5
$[-]$	$- 0.20]$	2%
a_c	$[2 \times 10^{-3}$	5
$[-]$	$- 25]$	8%
K_d	$[0.05$	5
$[-]$	$- 1.0]$	2%
K_s	$[10^{-6}$	5
$[\text{m s}^{-1}]$	$- 10^{-4}]$	7%

Table 1: Support of uncertain model parameters considered in the homogeneous test case, H_0 , and associated coefficients of variation (CVs).

Parameter	Support
$\sigma_Y^2, \sigma_{Y_{a_c}}^2,$ $\sigma_{Y_{SS}}^2$	[0.0 1 – 1.8]
$\lambda_Y, \lambda_{Y_{a_c}},$ $\lambda_{Y_{SS}}$ [m]	[25 – 50]

Table 2: Support of variance and correlation length characterizing the spatial random fields considered in the heterogeneous cases (H_1 , H_2 , and H_3).

	$\log K_s$	K_d	$\log a_c$	$\log S_s$	S_y
H_1	X	C	C	C	C
H_2	C	C	X	C	C
H_3	C	C	C	X	C

Table 3: Definition of the heterogeneous test cases. Quantities denoted by “X” are viewed as randomly heterogeneous and spatially correlated fields (with variance and integral scale listed in Table 2). Uncertain parameters denoted by “C” are considered as *i.i.d.* random variables within the supports listed in Table 1.

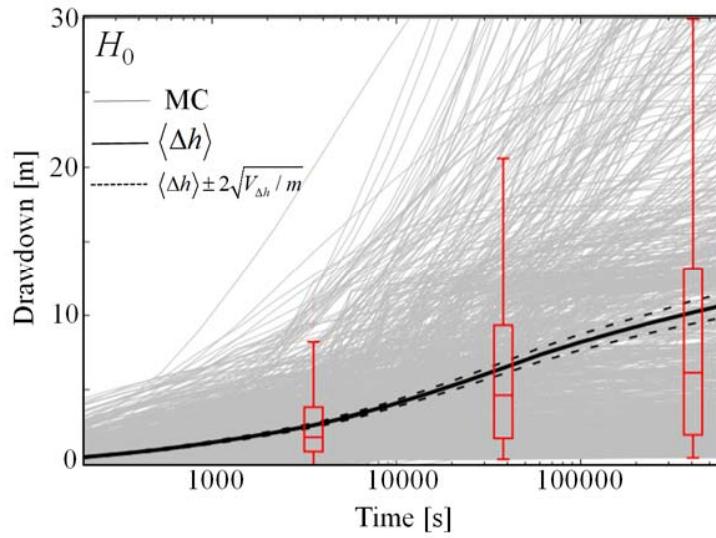


Figure 1. Temporal evolution of drawdown at point A (located at a radial distance from the well equal to 10 m and at the same depth as the well screened interval) computed for each MC realization (grey curves) in the homogeneous scenario (H_0). Ensemble mean drawdown (black continuous curve), its 95% Confidence Intervals (black dashed curves) and box-plots at three selected times (in red) are also depicted.

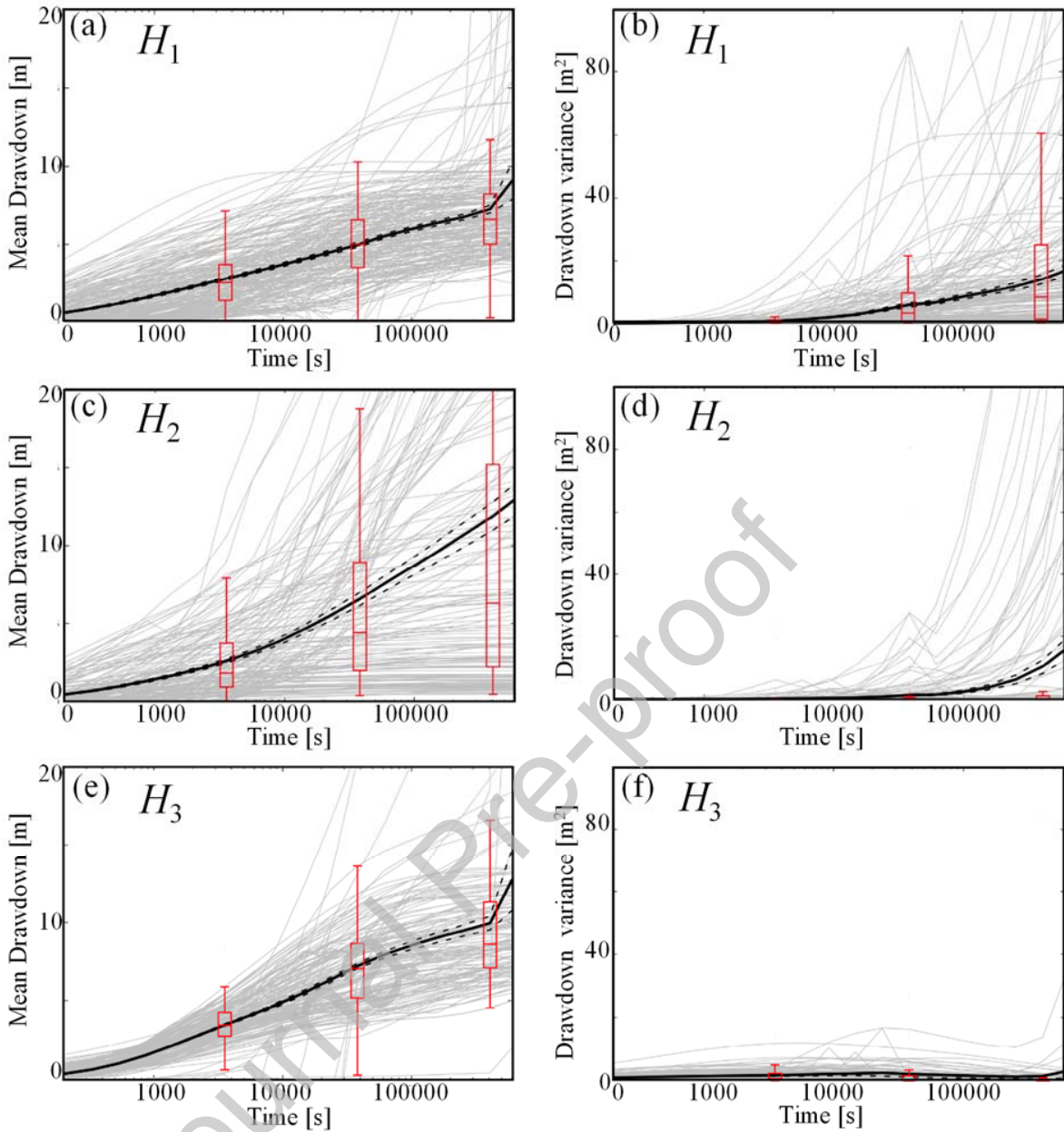


Figure 2. Temporal evolution of $\mu_{\Delta h, k}$ (left column) and $\sigma_{\Delta h, k}^2$ (right column) evaluated at point A for each set k of input parameters (grey curves) in the heterogeneous scenarios. Average curves computed across the full collection of parameter values (black continuous curves) and their 95% Confidence Intervals (black dashed curve) as well as the box plots evaluated at three selected times (in red) are also depicted.

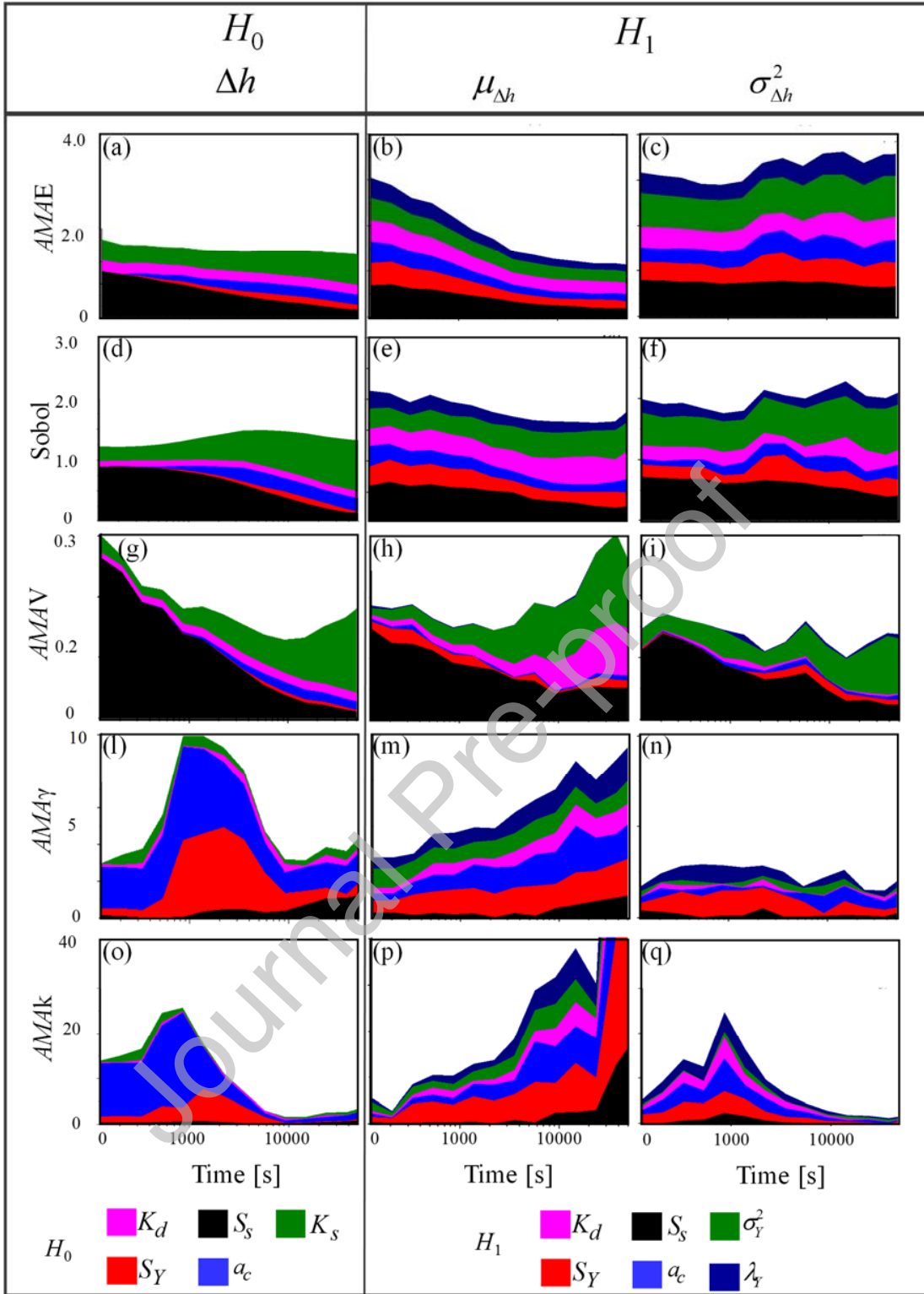


Figure 3. Temporal evolution of $AMAE$, Sobol', $AMAV$, $AMA\gamma$ and $AMAk$ indices associated with (i) Δh for H_0 (first column), (ii) $\mu_{\Delta h}$ for H_1 (second column) and (iii) $\sigma_{\Delta h}^2$ for H_1 (third column).

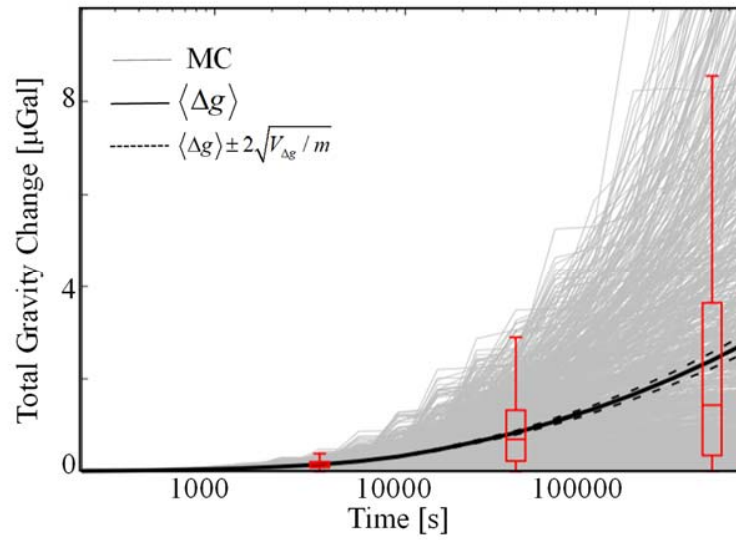


Figure 4. Temporal evolution of the total gravity change computed for each MC realization (grey curves) in the homogeneous scenario. Ensemble mean gravity change (black continuous curve), its 95% Confidence Intervals (black dashed curves) and box-plots at three selected times (in red) are also depicted.

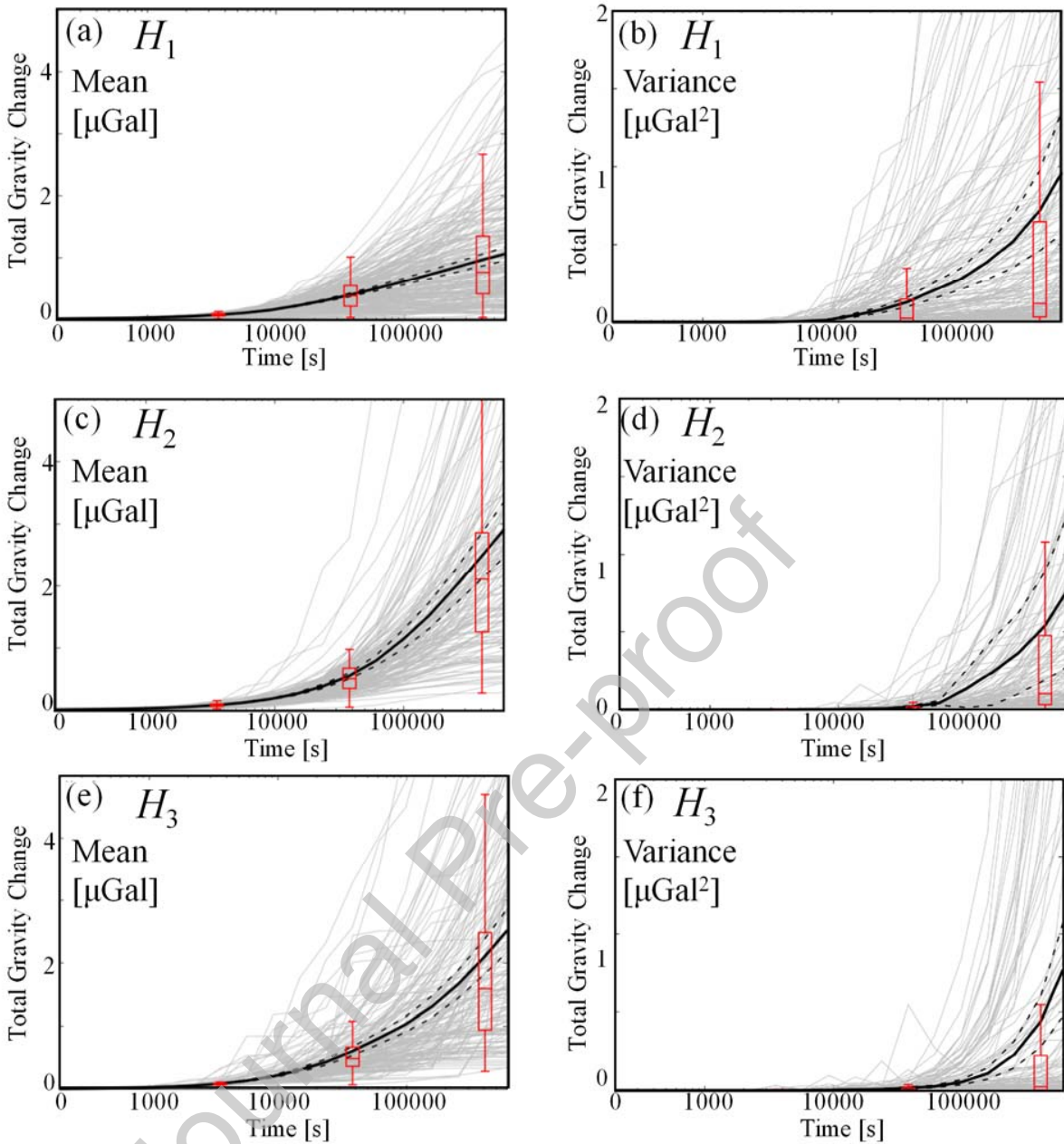


Figure 5. Temporal evolution of $\mu_{\Delta g,k}$ (left column) and $\sigma_{\Delta g,k}^2$ (right column) evaluated for each set k of input parameters (grey curves) in the heterogeneous scenarios. Average curves computed across the full collection of parameter values (black continuous curves) and their 95% Confidence Intervals (black dotted curve) as well as the box plots evaluated at three selected times (in red) are also depicted.

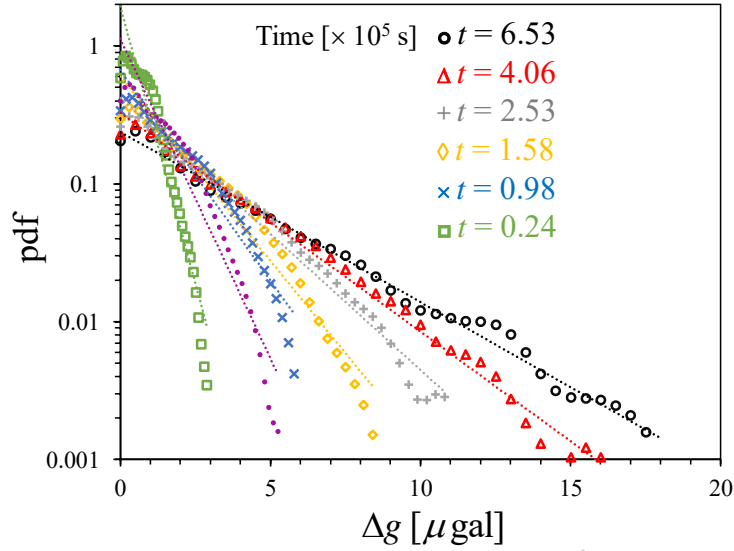


Figure 6. Sample pdf of Δg at selected times for H_0 (symbols). Exponential fitted models (dashed curves) are also shown for comparison.

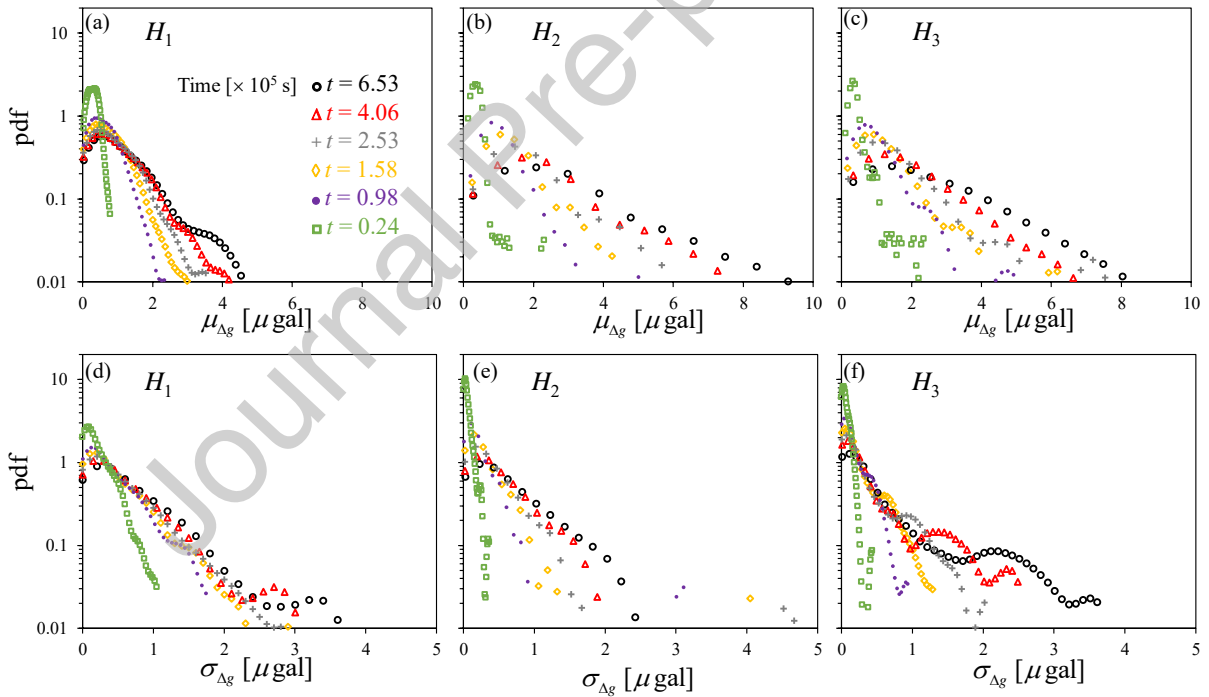


Figure 7. Sample pdf of $\mu_{\Delta g}$ (top) and $\sigma_{\Delta g}$ (bottom) at selected times for the heterogeneous scenarios (symbols).

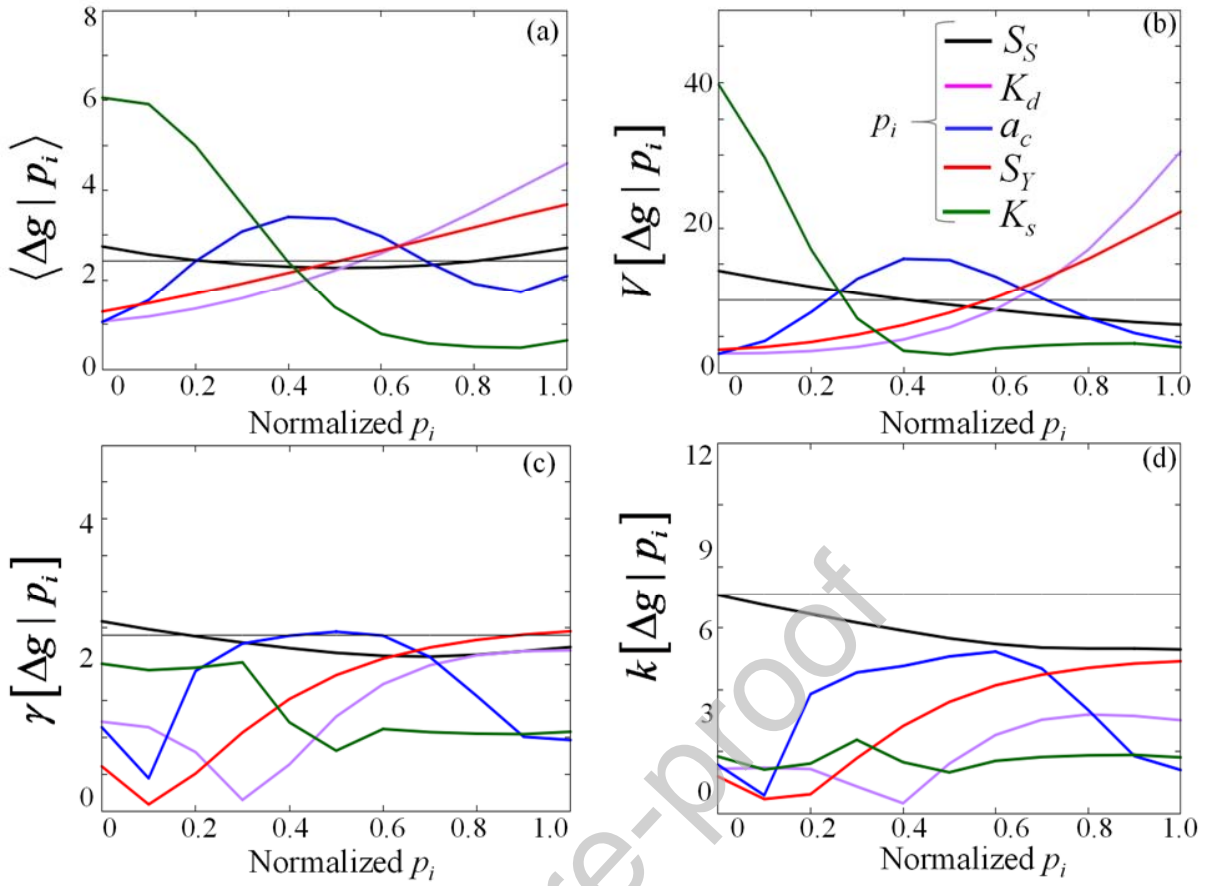


Figure 8. Conditional (a) mean, (b) variance, (c) skewness, and (d) kurtosis of Δg versus normalized model parameters p_i at time $t = 7$ days for H_0 . Corresponding unconditional moments are also shown (horizontal lines).

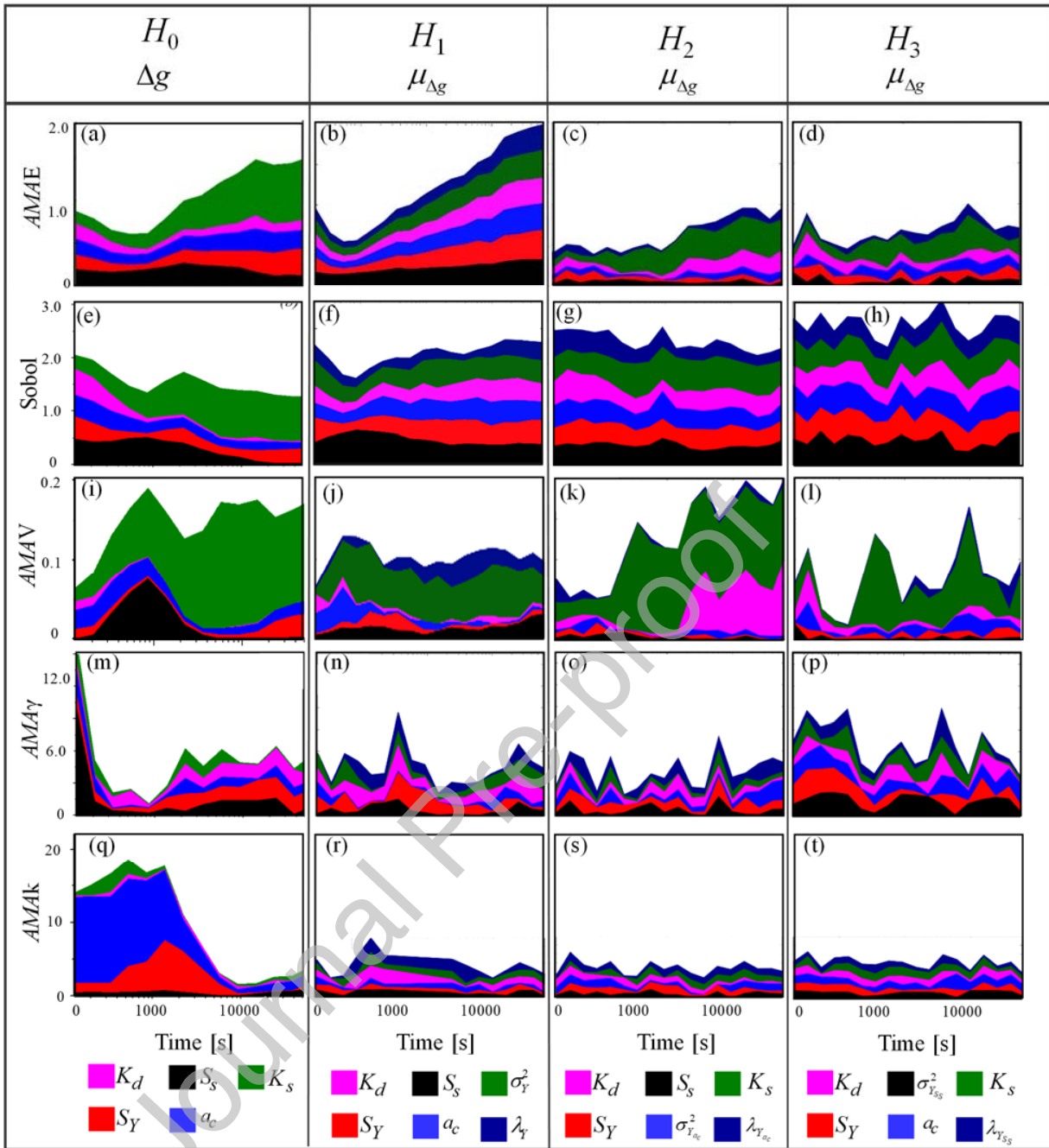


Figure 9. Temporal evolution of AMAE, Sobol', AMAV, AMA γ and AMA κ indices associated with (i) Δg for H_0 (first column), and (ii) $\mu_{\Delta g}$ for H_1 (second column), H_2 (third column), and H_3 (last column).

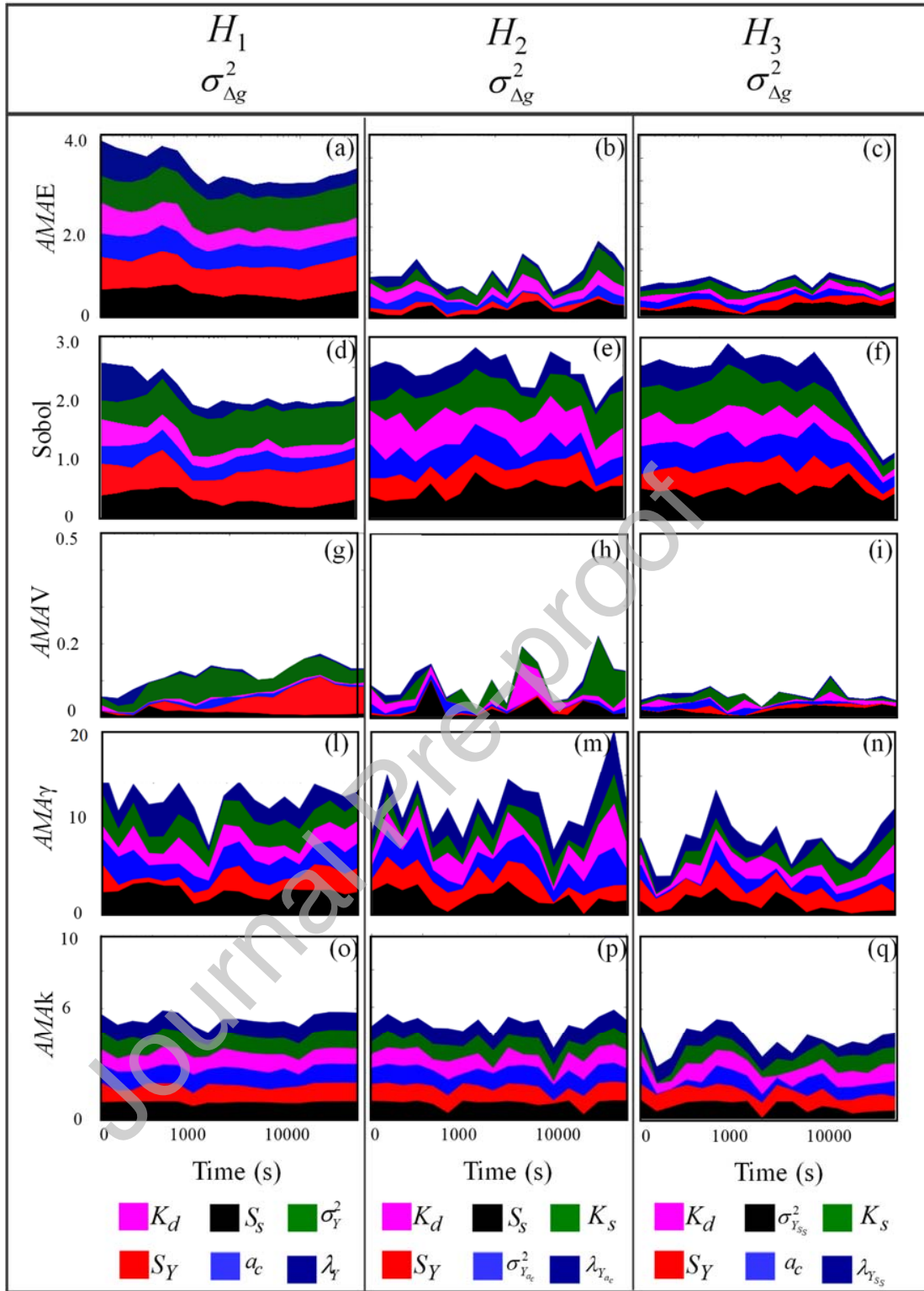


Figure 10. Temporal evolution of AMAE, Sobol', AMAV, AMA γ and AMA κ associated with $\sigma_{\Delta g}^2$ for H_1 (first column), H_2 (second column), and H_3 (third column).